Rheol Acta (2006) 45: 741–753
DOI 10.1007/s00397-005-0038-2

ORIGINAL CONTRIBUTION

Jun Wang
Sachin Velankar

Strain recovery of model immiscible blends: effects of added compatibilizer

Received: 7 January 2005
Accepted: 25 August 2005
Published online: 10 December 2005

J. Wang · S. Velankar (✉)
Department of Chemical Engineering,
University of Pittsburgh, Pittsburgh, USA
E-mail: velankar@pitt.edu

Abstract The effect of added compatibilizer on the strain recovery of model immiscible blends after cessation of shear was studied. Blends were composed of polyisobutylene drops (up to 30% by weight) in a polydimethylsiloxane matrix, with viscosity ratio (viscosity of the drops relative to the matrix viscosity) ranging from 0.3 to 1.7. Up to 1% by weight of a PIB-PDMS diblock copolymer was added as compatibilizer. The ultimate recovery recorded after reaching steady-shear conditions increased significantly due to added compatibilizer. Furthermore, the compatibilizer also slowed down the kinetics of the recovery; however, unlike uncompatibilized blends, the recovery could no longer be captured by a single retardation time. The largest increase in ultimate recovery due to compatibilizer occurred at the lowest viscosity ratio. In contrast, the greatest slowing down of the recovery due to compatibilizer occurred at the highest viscosity ratio. The rheological data by themselves are insufficient to reach a definitive conclusion about the mechanism of compatibilizer action. The results are consistent with the effects of flow-induced gradients in compatibilizer concentration. An alternative constitutive modeling approach that captures compatibilizer effects in terms of an interfacial dilational elasticity can reproduce the recovery curves qualitatively, but some predictions of the model contradict experimental results.

Keywords Immiscible blends · Compatibilizer · Creep recovery · Drop deformation · Interfacial tension

Introduction

Immiscible homopolymers are often blended mechanically to obtain blends with properties significantly superior to those of the component polymers. The creep recovery of such blends was studied in the previous paper, henceforth referred to as I. Surface-active compatibilizers are commonly added to such blends to improve blending of the immiscible phases and to improve the mechanical properties of the resulting blends. This paper continues previous research on the effect of such compatibilizers on the rheological properties of two-phase blends (Velankar et al. 2001a, b, 2004a; Van Hemelrijck et al. 2004). Following the philosophy of keeping bulk rheology as simple as possible in order to focus on interfacial effects, all experiments are conducted on "model" blends of nearly-Newtonian polymer melts. Moreover, at sufficiently large concentrations, the compatibilizer can modify the rheological properties of the bulk phases. In order to avoid this complication, experiments are restricted to blends with only small amounts of compatibilizer (1 wt% or less) at which their effects on bulk rheology are negligible (Velankar et al. 2004a).

Our previous research with such model compatibilized blends was restricted to droplet-matrix blends

with 10 wt% of the drop phase, with the ratio of the viscosity of drops to that of the matrix ranging 0.1–2.7 (Velankar et al. 2001a, b, 2004a; Van Puyvelde et al. 2002; Van Hemelrijck et al. 2004). While addition of the compatibilizer was found to reduce the mean drop size of the blends significantly, the primary concern was not the decrease of drop size; the primary focus was instead on the rheological properties of compatibilized blends. The following observations were made previously:

- Addition of compatibilizer increased the zero-shear viscosity of blends slightly at all viscosity ratios (Velankar et al. 2004a).
- The effect of the compatibilizer on the elastic properties was more complex: at low viscosity ratios, the compatibilizer did not affect the terminal relaxation time, but increased N_1 significantly. At high viscosity ratios, the observations were exactly reversed: the terminal relaxation time increased greatly, but N_1 was not affected by compatibilizer (Velankar et al. 2004a).
- At very small amounts of added compatibilizer (0.02% by weight or lower), the dynamic mechanical properties of the blends showed two relaxations (evident as two shoulders in the G′ vs. frequency curves) (Van Hemelrijck et al. 2004). The faster of the two relaxations was present even in uncompatibilized samples and was attributed to shape relaxation of the drops. The slower relaxation was present only in compatibilized samples and speeded up as the amount of compatibilizer increased, as was also observed previously (Riemann et al. 1997). As a consequence of this speeding up of the slow process, the two processes merged, and only a single relaxation was evident in blends with large amounts of compatibilizer (Velankar et al. 2001b, 2004a). Interfacial viscoelasticity due to the added compatibilizer was deemed to be responsible for the slower relaxation (Riemann et al. 1997; Jacobs et al. 1999).

The previous research was mainly concerned with dynamic oscillatory behavior, and with the rheological properties after reaching steady-shear conditions. Here we consider transient flow conditions. The goal of this research is to address the following questions: How does a small amount of surfactant affect the creep recovery of droplet-matrix blends? In particular, considering the opposite effects of viscosity ratio on N_1 and on the terminal relaxation time of compatibilized samples, how does the effect of the surfactant vary with viscosity ratio? Furthermore, considering that samples with very small amounts of compatibilizer can show two relaxation times (Riemann et al. 1997; Van Hemelrijck et al. 2004), does their creep recovery show two retardation times as well?

Experimental

The details of the materials were provided previously. Briefly, the blends were composed of PIB as the drop phase and PDMS as the matrix phase with properties described in I. A diblock copolymer of PIB (M_w = 6,150 g/mol) and PDMS (M_w = 8,000 g/mol) was added as compatibilizer. This same diblock was used by Velankar et al. (2001b, 2004a). As in I, we studied three weight% of the dispersed phase PIB (10, 20 and 30%), and three viscosity ratios (0.29, 1.1 and 1.7). Compatibilizer loadings range 0–1 wt%, with most experiments being conducted with 0.2 wt% of compatibilizer. Note that throughout this paper the compatibilizer amount is quoted as a percentage of the total weight of the blend [and not as the percent of the dispersed phase as was done previously (Velankar et al. 2001b, 2004a)].

Samples were prepared by mixing the diblock into the PIB and then dispersing this mixture into the PDMS matrix. All experimental techniques are identical to those in I. In particular, the shear history of Fig. 1a in I was used to study strain recovery after cessation of steady shear, as described in the following Sect. 3.1.

Experimental observations

Recovery after cessation of steady shear

The creep recovery behavior of uncompatibilized blends was discussed in I. The recovery of compatibilized blends shows many of the same features, at least qualitatively. These are summarized first:

- The recovery curves of compatibilized blends are qualitatively similar to those of uncompatibilized ones (see Fig. 2 in I). In particular, most of the recovery prior to 0.1 s is attributable to the recovery of the matrix phase PDMS. We can therefore extract the interfacial contribution to the recovery by simply subtracting the volume average of the recovery of the components from that of the blends (Eq. 13 in I).
- Most compatibilized blends show a slight reversal of recovery similar to that seen for uncompatibilized blends (see Fig. 1b in I). The amount of strain reversal is comparable to that for blends without compatibilizer (~0.02 for recovery from a steady-shear morphology), but the reversal takes a much longer time for compatibilized blends.
- Upon stepping down the shear stress from 480 to 120 Pa (as per the shear history of Fig. 1a in I), the ultimate recovery of the blends with 10% drop phase increases significantly. A plot of the ultimate recovery versus the total strain applied at 120 Pa looks very similar to Fig. 3a in I. This may be attributed to an

increase in drop size by shear-induced coalescence (Velankar et al. 2001b, 2004a).
– As in I, for blends with 10% drops, dynamic oscillatory frequency sweep experiments were conducted after each recovery experiment. As observed previously (Velankar et al. 2001b, 2004a), at most levels of compatibilizer, only a single shoulder was evident in the G′ versus frequency curve (see exception below). The relaxation time of this shoulder increased upon shearing at 120 Pa. Comprehensive examples of such results on similar blends have been published previously [see Fig. 2 in (Velankar et al. 2004a)].
– For blends with 20 or 30% drops, a plot similar to Fig. 3b in I is obtained, i.e., at very short shearing times, the ultimate recovery is large and then decreases to its steady-state value. Once again, we propose no mechanism to explain this observation.

The differences between blends with and without compatibilizer are now considered. Figure 1 plots the frequency sweep results of the blends with 10% drops and $p = 1.1$. Such curves were analyzed extensively in our previous publications on this PIB/PDMS system with the same compatibilizer (Velankar et al. 2001b, 2004a). In those publications the smallest block copolymer concentration studied was 0.05 wt% of the total, and we had concluded that the compatibilized blends showed frequency sweep data that were qualitatively identical to those of uncompatibilized ones; specifically, only one shoulder was evident in the G′ versus ω data. In light of later data on a somewhat different compatibilized blend system (Van Hemelrijck et al. 2004), we reexamined the present system at even lower concentrations than previously and indeed found a weak second shoulder developing at very low frequencies. The second shoulder was most clearly visible at the lowest compatibilizer loading of 0.01%, immediately after preshearing at 480 Pa (Fig. 1). As the sample was sheared at 120 Pa, the shoulder at higher frequency moved to lower frequency, and merged with the low-frequency shoulder. As a result, two separate shoulders were no longer distinguishable after the sample reached steady-shearing conditions at 120 Pa. The principal conclusion, therefore, is that some compatibilized blends can show two relaxation processes, hence one of the questions was posed in the Introduction: can they also show two distinct retardation processes?

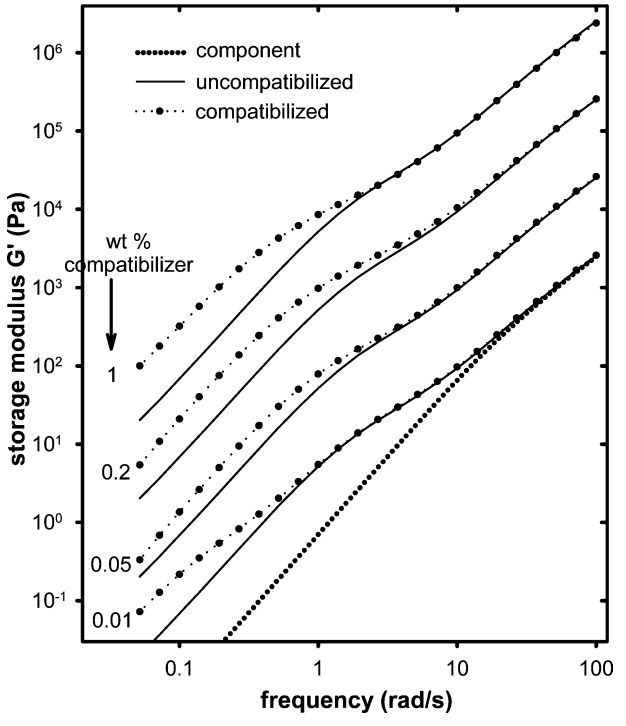

Fig. 1 Dynamic oscillatory G′ of compatibilized blends with $p = 1.1$ and 10 wt% drops at the end of preshearing at 480 Pa. The data for each compatibilizer concentration are shifted upwards from the previous one by one decade for clarity; the data at 0.01% compatibilizer are not shifted. The G′ of the uncompatibilized blend is shown alongside each curve for comparison. The component contribution (*dotted line*) is the Palierne model with interfacial tension set to zero

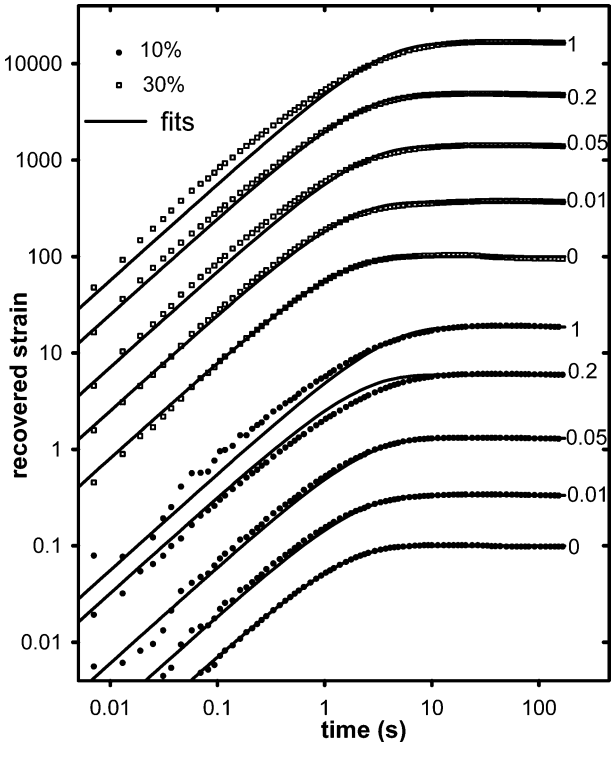

Fig. 2 Recovery of blends with viscosity ratio 1.1, 10 or 30% drops, and various levels of compatibilizer. Each curve is shifted upwards by a half-decade with respect to the previous one for clarity; the lowest dataset is not shifted. *Solid lines* are best fits of single exponential recovery kinetics to the data for time > 0.02 s

In what follows, only the recovery after reaching steady-shearing conditions at 120 Pa will be discussed. Figure 2 plots the recovery of the blends with a viscosity ratio of 1.1, 10 or 30 wt% drops, and various amounts of compatibilizer. Two features are noteworthy. Firstly, the addition of compatibilizer increases the ultimate recovery significantly (this is shown more clearly in Fig. 3a). Secondly, in contrast with the uncompatibilized biends in I, single-exponential kinetics can no longer accurately capture the recovery of blends with large amount of compatibilizer: the solid lines, which are fits to single exponential kinetics,

$$\gamma = \gamma_\infty[1 - \exp(-t/\lambda)] \quad (1)$$

fit the data poorly. Interestingly enough, while the two relaxation processes are most clearly visible in dynamic oscillatory experiments at the *lowest* compatibilizer level [Fig. 1 as well as (Van Hemelrijck et al. 2004)], the greatest deviations from single exponential kinetics occur at the *highest* compatibilizer levels. We have therefore immediately answered one of the questions posed in the Introduction: the recovery from steady shearing of compatibilized blends cannot be captured by a single-retardation time.

Since recovery is not a single-exponential process, its rigorous quantitative analysis requires converting the recovered strain versus time curves into a retardation spectrum. This is an ill-posed problem generally requiring nonlinear regularization methods, but these were not attempted here. In the remainder of this paper, we will therefore persist with single-exponential fits to obtain a single retardation time for each curve. While the fits are poor at high compatibilizer fractions, these approximate retardation times are useful practically since they capture the gross kinetics of the recovery process (e.g. they track the time for completing half of the recovery very well) and hence allow us to comment on the effect of compatibilizer. As in I, these retardation times are multiplied by the shear rate prior to recovery to render them dimensionless. Thus to summarize, as in I, the recovery from steady-shearing conditions will be characterized by only two parameters: the ultimate recovery and the dimensionless retardation time.

These two quantities are plotted in Fig. 3 for the blends with viscosity ratio 1.1. The compatibilizer is seen to increase the ultimate recovery of the blends as well as increase their dimensionless retardation time. The effect of compatibilizer is not subtle; the addition of as little as 0.2 wt% compatibilizer increases the ultimate recovery and the dimensionless retardation time by more than 50%. As mentioned above, the dimensionless retardation time is not rigorous at large compatibilizer loadings due to poor quality of fits. Yet, there is no doubt that it increases significantly; indeed the slower recovery kinetics of compatibilized blends is evident from Fig. 2 itself.

The effect of compatibilizers on blends with $p \neq 1$ is now considered. In the Introduction, it was mentioned that in previous research, two elastic properties: the terminal relaxation time after reaching steady shear (obtained from dynamic oscillatory experiments) and N_1 during steady shear were found to be affected differently by compatibilizer: the compatibilizer increased the terminal relaxation time only at high viscosity ratio, but the steady shear N_1 only at low viscosity ratio (Velankar et al. 2004a). Figure 4 examines the effect of viscosity ratio on two other elastic properties: the ultimate

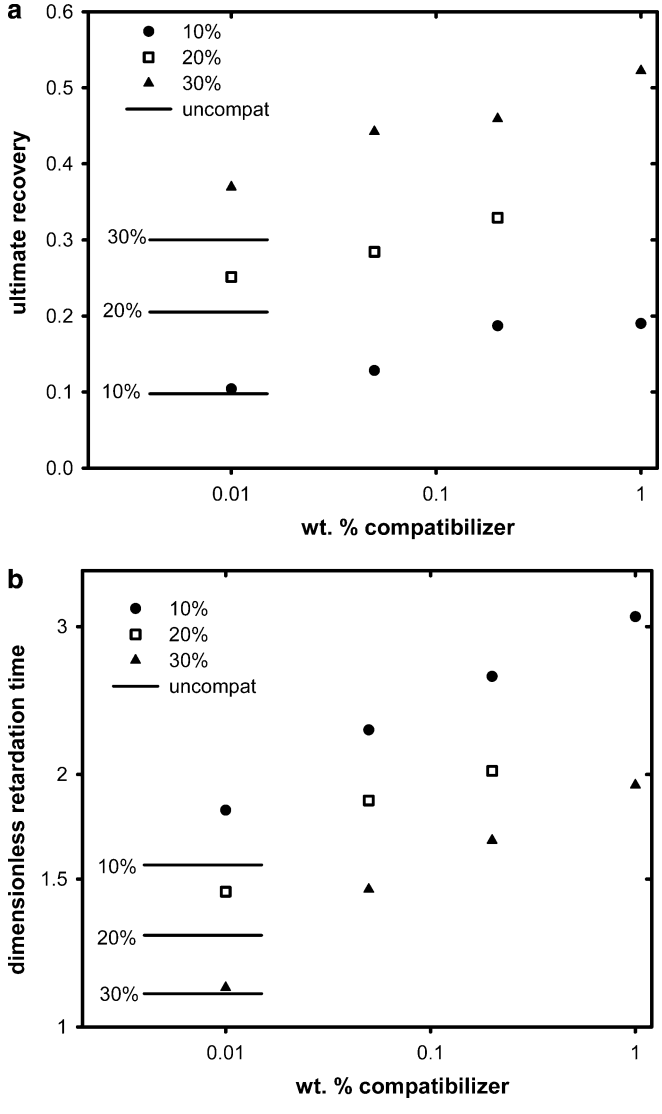

Fig. 3 Dependence on the concentration of compatibilizer of **a** ultimate recovery and **b** dimensionless retardation time, of blends with viscosity ratio 1.1, and 10, 20 or 30 wt% drops after reaching steady shear at 120 Pa. Note that **b** has both axes logarithmic. The retardation times at high compatibilizer content are approximate due to poor fits to the recovery curves

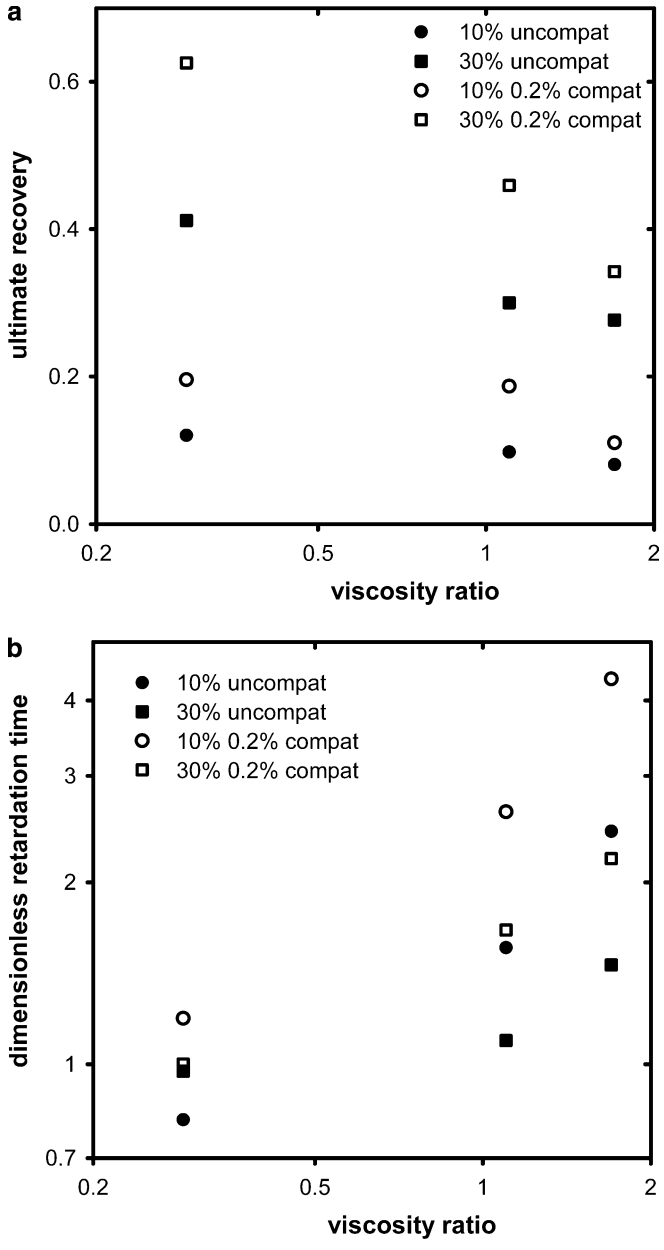

Fig. 4 Dependence on viscosity ratio of **a** ultimate recovery and **b** dimensionless retardation time, of blends with 10 or 30 wt% drops with and without compatibilizer after reaching steady shear at 120 Pa

recovery and the dimensionless retardation time after reaching steady-shear conditions. The effect of compatibilizer on γ_∞ is largest at low p but modest at high p; in this regard creep recovery seems to behave like N_1, at least qualitatively. On the other hand, the effect of compatibilizer on the dimensionless retardation time is largest at high p but modest at low p. Thus, in regard to the dimensionless retardation time, creep recovery behaves qualitatively similar to the dimensionless relaxation time.

Finally, the effects of volume fraction at fixed viscosity ratio (not plotted) are similar to those of uncompatibilized blends discussed in I:

- The ultimate recovery under steady-shear conditions increases with volume fraction of the drops at all compatibilizer levels. As in uncompatibilized samples, the increase is nearly proportional to ϕ, or slightly faster.
- The retardation time reduces with increasing volume fraction of drops at all compatibilizer levels (with the sole exception of the uncompatibilized sample at $p = 0.29$ as shown in Fig. 5b in I).

Recovery after cessation of brief shearing

As discussed in I, in blends without compatibilizer, recovery is driven by the deformation and orientation of drops. Steady-state deformation of drops increases with capillary number, hence the ultimate recovery increases with capillary number. However, only modest deformations can be realized under steady-shear conditions because the steady-state Ca that can be applied is limited to values below the critical Ca for breakup of drops. Under transient flow conditions, however, very large deformations can be realized. Vinckier et al. (1999a) considered recovery of blends with such highly deformed drops. Blends were presheared at low stresses to allow large drops to be formed by flow-induced coalescence. They were then sheared briefly at high Ca to deform the drops, and subsequent recovery was measured. Owing to the much larger deformations achievable, ultimate recovery was found to be much larger after such transient shearing. Here we examine effects of compatibilizer on strain recovery under similar transient shearing.

Blends with 30 wt% drops, $p = 1.1$, and either 0 or 0.2% compatibilizer were subjected to the transient shear history of Fig. 5a. Samples were sheared for 2,000 strain units at 30 Pa, which is sufficient for them to be close to their steady state. They were then sheared at 120 Pa for brief periods denoted by t_s, with the corresponding strains denoted by γ_s. The subsequent recovery curves are plotted in Fig. 5b. Comparing the recovery curves for the uncompatibilized blend (solid circles) at various values of t_s, it is immediately evident that the time required to complete the recovery first increases and then decreases with increasing t_s (i.e. with increasing γ_s). The same is true for ultimate recovery as shown more clearly in the plot of γ_∞ versus γ_s in Fig. 6; this figure resembles previous data by Vinckier (1999a).

Upon addition of compatibilizer, the most obvious effect evident in Fig. 5b is that the compatibilizer increases the ultimate recovery at all values of t_s. This is shown more clearly in Fig. 6. A second, more subtle, difference is that at very long times, a slow retardation process is evident at small t_s. This is most clearly visible

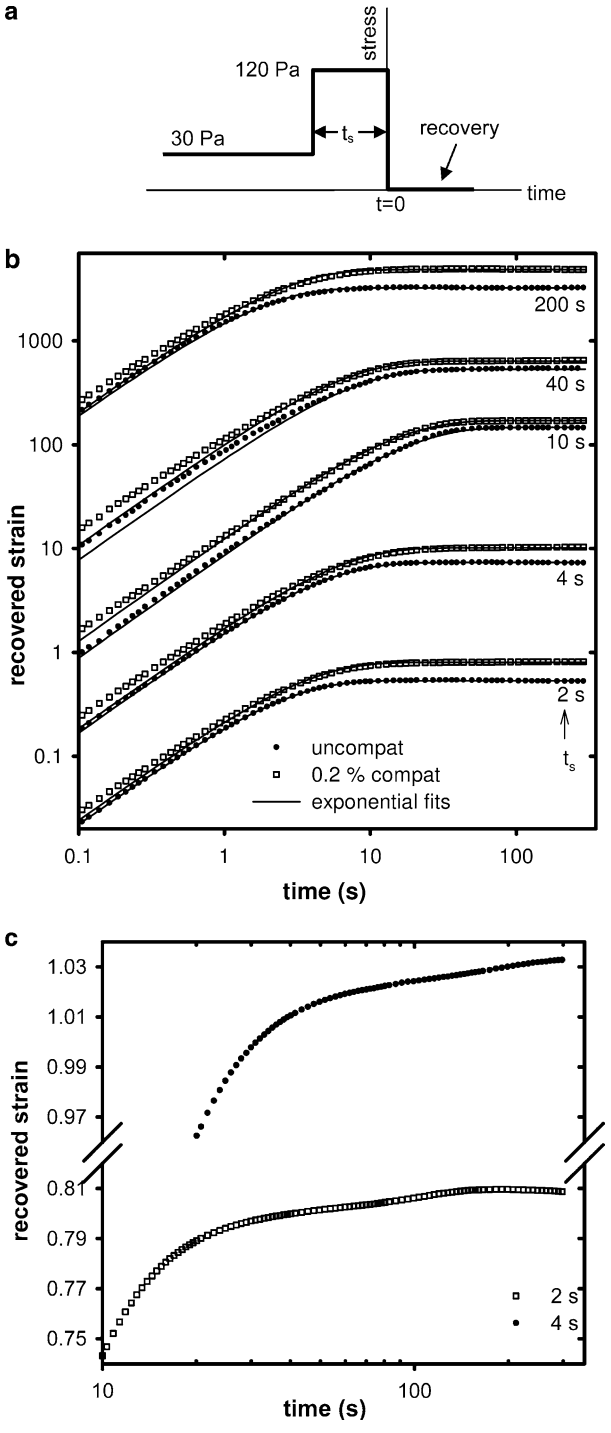

Fig. 5 Recovery of blends after transient shear. **a** Schematic of transient shear experiment. **b** Recovery at various values of t_s with and without compatibilizer. Each pair (uncompatibilized and 0.2% compatibilized) is shifted upwards by a decade with respect to the previous t_s value; the pair at $t_s = 2$ s is not shifted. At any given value of t_s, the uncompatibilized and the compatibilized data are not shifted with respect to each other. **c** Magnified views of the recovery curves of compatibilized blends at $t_s = 2$ s and $t_s = 4$ s. Note that the *y*-axis in **c** is linear

at $t_s = 2$ and 4 s for the 0.2% compatibilized sample (Fig. 5c) but similar slow retardations were evident at other values of t_s and at other compatibilizer levels. This slow process is quite weak: the ultimate recovery during this process is less than 0.02. The slow retardation is no longer evident when t_s exceeds about 20 s.

Finally, as in the previous section, we attempted to fit the recovery curves to the single-exponential kinetics (1). These fits were quite poor for both the compatibilized as well as uncompatibilized sample, especially around $t_s \approx 40$ as shown in Fig. 5b. Therefore, while the fits are still shown in Fig. 5b, the resulting best-fit retardation times are not interpreted any further.

Discussion and possible mechanisms

Review of uncompatibilized blend recovery

We first review the recovery of uncompatibilized blends under steady and transient conditions. The linear viscoelastic theory for the recovery of uncompatibilized blends from steady shearing (Vinckier et al. 1999b) was reviewed in I. Briefly, recovery is driven by the deformation and orientation of drops along the flow direction. Under steady-shear conditions, the ultimate recovery and the dimensionless retardation time are both proportional to the Ca prior to recovery. Both these quantities also have additional dependences on viscosity ratio and volume fraction of the drops.

The recovery upon transient shearing is more complex since the deformations can be much larger. As discussed by Vinckier et al. (1999a), the data of Fig. 6 can be divided into three regions. On the left of the maximum ($\gamma_s < 10$), the applied stress deforms the drops, and strain recovery is completed when deformed droplets retract, hence, increasing γ_s increases γ_∞. On the right of the maximum ($10 < \gamma_s < 60$) on the other hand, the deformation creates highly elongated cylinders, and recovery is completed when these cylinders break by capillary instabilities. Increasing γ_s creates cylinders with smaller diameter, thus reducing the time for capillary instabilities, and hence reducing γ_∞. Finally, at very high shearing times ($\gamma_s > 100$), cylinder breakup is completed during the shearing itself. Thus when shearing is stopped, the morphology consists of drops that are much smaller, and hence less deformed, than the original drops. Recovery involves retraction of these drops, and since their size changes very slowly with strain, γ_∞ is nearly independent of γ_s.

Compatibilized blends

As in previous publications, we will consider the compatibilizer to act only as a surfactant that reduces the

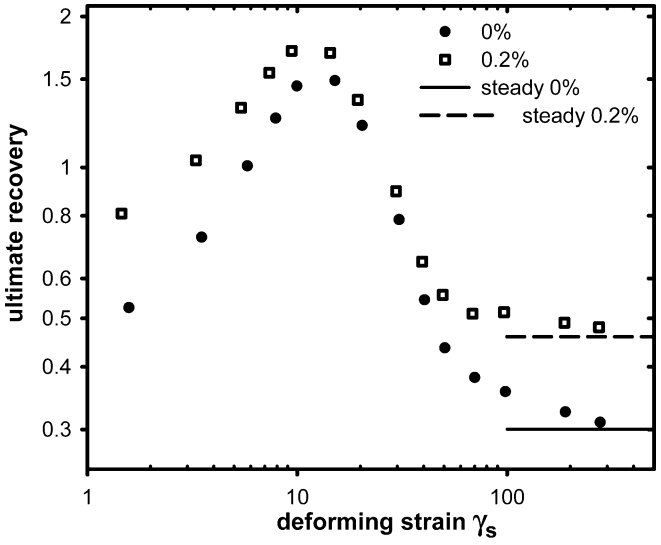

Fig. 6 Ultimate recovery of blends with p = 1.1 presheared at 30 Pa for 2,000 strain units, followed by 120 Pa for strains plotted on the x-axis. Horizontal lines are the γ_∞ from steady shearing at 120 Pa

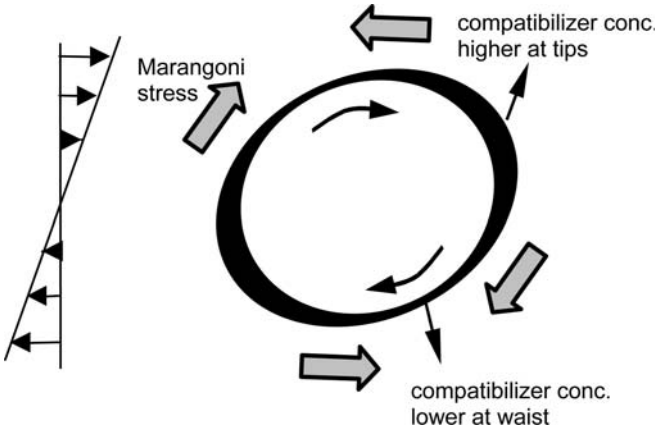

Fig. 7 Schematic of physical picture of a single drop with compatibilizer under shear flow (Velankar et al. 2004a). Local interfacial concentration of compatibilizer is shown schematically by the thickness of the black boundary of the drop

equilibrium interfacial tension between the phases. If the compatibilizer is highly soluble in the bulk phases, and has a very high diffusivity, all locations on the interface are guaranteed to have the same equilibrium value of compatibilizer concentration at all times. However, a rough calculation in a previous publication suggests that the compatibilizer used here is likely to have a very low diffusivity (Velankar et al. 2001b). The same is expected to be true for most compatibilizers owing to their high molecular weights. In that case, the coupling between flow, interfacial deformation, and the compatibilizer concentration must be considered: flow can induce a change in the average concentration of compatibilizer as well as gradients in compatibilizer concentration on the interface that are not erased by rapid diffusion. On the basis of the numerical simulations exploring this coupling (Stone and Leal 1990; Milliken and Leal 1994; Pawar and Stebe 1996; Li and Pozrikidis 1997), a physical picture was proposed in previous publications to interpret the rheological effects of compatibilizer (Velankar et al. 2001b, 2004a). To summarize briefly, the applied flow convects the compatibilizer to tips of the drops (Fig. 7). Therefore, the tips have a higher concentration of compatibilizer, and hence a lower interfacial tension, than the waist of the drops. This lowers the capillary pressure of the tips, but also induces a Marangoni stress as shown in Fig. 7. A variety of experimental evidence supporting this physical picture was cited previously (Velankar et al. 2004a). In the following, we will consider the implications of such a nonuniform interfacial tension for the recovery process.

The nonuniform interfacial tension can affect recovery indirectly and directly. The indirect effect is that the initial deformation of compatibilized drops, i.e., the deformation at the instant recovery begins, is expected to be affected by compatibilizer. The effect of compatibilizer on deformation is not straightforward: numerical simulations show that, depending on various parameters values (viscosity ratio, capillary number, and properties of the surfactant), compatibilizers can increase or decrease steady-state deformation (Stone and Leal 1990; Pawar and Stebe 1996; Li and Pozrikidis 1997). The direct effect of nonuniform interfacial tension on recovery is that the stresses driving retraction of the drops (and hence recovery of the blend) are modified. For example, as a compatibilized drop retracts, the average compatibilizer concentration on its surface increases, thus, reducing the average interfacial tension, and hence also reducing the capillary pressure driving recovery. This is expected to slow the recovery of compatibilized blends. In contrast, the Marangoni stress is an additional stress driving the recovery of compatibilized drops, and hence is expected to increase the ultimate recovery and accelerate the recovery. Clearly, if Fig. 7 is indeed the relevant physical picture to interpret rheological effects of compatibilizer, its implications to the recovery process are quite complex: whether recovery increases or decreases and whether it is slower or faster depends on the parameters mentioned above.

Owing to the high volume fraction of drops, the blends scatter light strongly, and in situ flow visualization is difficult. We did attempt flow visualization using a Linkam CSS 450 shear cell. While we were able to confirm that compatibilized blends had considerably smaller drops, we were unable to reach any firm conclusions about their dynamics. For example, we were not even able to ascertain with confidence whether compatibilized drops are more or less deformed during steady shearing.

In the absence of even qualitative information from flow visualization, we are unable to speculate on the exact mechanism by which the compatibilizer increases the strain recovered and the retardation time.

Finally, we discuss possible reasons for the slow retardation process evident in compatibilized blends at small t_s in Fig. 5c. Recent simulations examined the shear-induced deformation and the subsequent retraction of a surfactant-laden drop (Velankar et al. 2004b). Drops were deformed by shear strains of 1 or 5 strain units (vs. ~1.6 and 3.5 strain units for the two samples in Fig. 5c). Drops without surfactant retracted exponentially; i.e., the deformation parameter decreased exponentially with time as expected (Luciani et al. 1997). Drops with small amount of surfactant retracted exponentially down to a certain deformation, and then retracted far more slowly. The results were explained in terms of nonuniform interfacial tension on the surface of the retracting drop: due to higher surfactant concentration (and lower interfacial tension) at the drop tips relative to the waist, at some time during retraction, the capillary pressure difference between the tips and the waist driving the retraction decreased and became negligible. Subsequent retraction was then driven by much weaker Marangoni stresses, and hence was much slower (Velankar et al. 2004b). The same mechanism can explain the slow retardation process of Fig. 5c: we speculate that in Fig. 5c, for $t > 100$ s, recovery is driven by weak Marangoni stresses only and hence occurs slowly. We emphasize once again that the strain associated with the slow retardation process is quite small (< 0.02) and hence likely to be of little practical relevance.

Constitutive modeling

The previous section sought to explain the effect of compatibilizer on the creep recovery in terms of the microscopic model of Fig. 7. In the absence of direct information about compatibilizer concentration gradients, or even about drop shapes, no firm comments about the mechanism could be made. An alternate approach, based upon a constitutive equation, is explored here. The chief idea is that the compatibilizer, or indeed any surfactant, gives the interface viscoelastic properties such as an interfacial modulus or an interfacial viscosity. The corresponding effects can be incorporated into a constitutive equation for the rheological properties of the droplet-matrix blend.

Constitutive equation

Oldroyd (1953) showed that for an emulsion whose interfaces could be described by their equilibrium interfacial tension alone,

$$\left(1 + \lambda_{F1}\frac{\mathrm{d}}{\mathrm{d}t}\right)\sigma = \eta_b\left(1 + \lambda_{F2}\frac{\mathrm{d}}{\mathrm{d}t}\right)\dot{\gamma}, \tag{2}$$

where λ_{F1} and λ_{F2} are the relaxation and the retardation times, respectively. All the three constitutive properties, η_b, λ_{F1}, and λ_{F2} can be related to the characteristics of the blend such as the drop size and interfacial tension. It was by integrating this equation that the Vinckier model (Eq. 2 in I) was derived (Vinckier et al. 1999b).

An equilibrium interfacial tension is often insufficient to characterize the mechanical properties of interfaces; often additional viscoelastic properties such as an interfacial modulus or an interfacial shear viscosity are necessary. For example, if a surfactant-laden interface at equilibrium is dilated, the surfactant concentration decreases, thus, increasing its interfacial tension. This can be described in terms of an interfacial dilation modulus β:

$$\beta = A\frac{\partial \alpha}{\partial A}, \tag{3}$$

where A is the area of the interface (Edwards et al. 1991). Indeed, all surfactant-laden interfaces must have a dilation modulus, and it can be related to the slope of the curve of interfacial tension versus interfacial surfactant concentration. The diffusion of surfactant from the bulk will eventually reduce the interfacial tension back to the equilibrium value, hence β is generally time (or frequency) dependent, but only the frequency-independent case will be considered here. Thus, we only treat the simplest case of blends whose interfaces have two mechanical properties: the equilibrium interfacial tension α and a frequency-independent interfacial dilation modulus, β.

Oldroyd (1955) and later Palierne (1990), showed that every additional interfacial viscoelastic property gives the emulsion an additional relaxation and an additional retardation time. Since the interface here has two mechanical properties, the corresponding emulsion has two relaxation times denoted by λ_{F1} and $\lambda_{\beta 1}$, and two retardation times denoted by λ_{F2} and $\lambda_{\beta 2}$. The linear viscoelastic constitutive equation of such a blend is (Oldroyd 1955)

$$\left(1+\lambda_{F1}\frac{\mathrm{d}}{\mathrm{d}t}\right)\left(1+\lambda_{\beta 1}\frac{\mathrm{d}}{\mathrm{d}t}\right)\sigma = \eta_{\mathrm{b}}\left(1+\lambda_{F2}\frac{\mathrm{d}}{\mathrm{d}t}\right)\left(1+\lambda_{\beta 2}\frac{\mathrm{d}}{\mathrm{d}t}\right)\dot{\gamma}. \tag{4}$$

The parameters λ_{F1}, λ_{F2}, $\lambda_{\beta 1}$, $\lambda_{\beta 2}$, and η_b have been related to the properties of the blend by Oldroyd (1955) (assuming Newtonian bulk phases) and by Palierne (1990) (assuming linear viscoelastic bulk phases). Here we will use explicit expressions for λ_{F1}, λ_{F2}, $\lambda_{\beta 1}$, and $\lambda_{\beta 2}$, derived from the Palierne model by Jacobs et al. (1999) These expressions have been provided in the

Appendix; here we only note that all the four times of interest can be written in the form as follows:

$$\lambda_i = \frac{\mathrm{R}\eta_\mathrm{m}}{\alpha} \times f\left(p, \phi, \frac{\beta}{\alpha}\right) \tag{5}$$

i.e., all the times λ_i are proportional to $\mathrm{R}\eta_\mathrm{m}/\alpha$. Here we are concerned with strain recovery following cessation of steady shear, we will define the corresponding dimensionless times as follows:

$$\lambda_i^* = \dot{\gamma}_0 \lambda_i = \mathrm{Ca} \times f\left(p, \phi, \frac{\beta}{\alpha}\right), \tag{6}$$

where $\dot{\gamma}_0$ is the shear rate prior to cessation of shear. It should be noted that the interfacial dilation modulus β does not appear independently in the equations in the Appendix, but only as a ratio β/α; this ratio, called the "surfactant elasticity", was denoted by E^* previously (Velankar et al. 2004b).

Integration of the constitutive equation with two-retardation processes

Expanding out (4)

$$\sigma + \left(\lambda_{F1} + \lambda_{\beta 1}\right)\frac{\mathrm{d}\sigma}{\mathrm{d}t} + \lambda_{F1}\lambda_{\beta 1}\frac{\mathrm{d}^2\sigma}{\mathrm{d}t^2} = \eta_\mathrm{b}\left[\frac{\mathrm{d}\gamma}{\mathrm{d}t} + \left(\lambda_{F1} + \lambda_{\beta 2}\right)\frac{\mathrm{d}^2\gamma}{\mathrm{d}t^2} + \lambda_{F2}\lambda_{\beta 2}\frac{\mathrm{d}^3\gamma}{\mathrm{d}t^3}\right]. \tag{7}$$

We will integrate this to obtain the strain recovery following cessation of steady shear (Fig. 8a) using Laplace transforms. It is algebraically easier to instead treat the recovery experiment as the subtraction of a creep experiment from the steady-state experiment as illustrated in Fig. 8. For the steady experiment Fig. 8b, obviously

$$\dot{\gamma}_0 = \frac{\sigma_0}{\eta_\mathrm{b}} \text{ and hence } \gamma = \frac{\sigma_0}{\eta_\mathrm{b}} t. \tag{8}$$

For the creep experiment, we can arbitrarily choose the strain at $t = 0$ to be zero. Since the sample in Fig. 8c has not experienced any stress up to $t = 0$, all higher derivatives of the stress and the strain are also zero at $t = 0$:

$$\sigma|_{t=0} = 0; \quad \dot{\sigma}|_{t=0} = 0; \quad \gamma|_{t=0} = 0; \quad \dot{\gamma}|_{t=0} = 0; \quad \ddot{\gamma}|_{t=0} = 0. \tag{9}$$

Applying Laplace transforms to (7)

$$\Sigma + \left(\lambda_{F1} + \lambda_{\beta 1}\right)\left[s\Sigma - \sigma|_{t=0}\right] + \lambda_{F1}\lambda_{\beta 1}\left[s^2\Sigma - s\sigma|_{t=0} - \dot{\sigma}|_{t=0}\right] = \eta_\mathrm{b}\left[s\Gamma - \gamma|_{t=0} + \left(\lambda_{F2} + \lambda_{\beta 2}\right)\left\{s^2\Gamma - s\gamma|_{t=0} - \dot{\gamma}|_{t=0}\right\}\lambda_{F2}\lambda_{\beta 2} \times \left\{s^3\Gamma - s^2\gamma|_{t=0} - s\dot{\gamma}|_{t=0} - \ddot{\gamma}|_{t=0}\right\}\right]. \tag{10}$$

Here $\Sigma(s)$ and $\Gamma(s)$ are the Laplace transforms of $\sigma(t)$ and $\gamma(t)$, respectively. Substituting the initial conditions and inserting $\Sigma = \sigma_0/s$ as the Laplace transform of the $\sigma(t)$ in Fig. 8c,

$$\Gamma = \frac{\sigma_0}{\eta_\mathrm{b}}\frac{1}{s^2}\frac{1 + \left(\lambda_{F1} + \lambda_{\beta 1}\right)s + \lambda_{F1}\lambda_{\beta 1}s^2}{1 + \left(\lambda_{F2} + \lambda_{\beta 2}\right)s + \lambda_{F2}\lambda_{\beta 2}s^2}. \tag{11}$$

Inverting this, the strain as a function of time for the retardation experiment is obtained:

$$\gamma = \frac{\sigma_0}{\eta_b}t + \frac{\sigma_0}{\eta_b} \times \left[\lambda_{F1} + \lambda_{\beta 1} - \lambda_{F2} - \lambda_{\beta 2} + \frac{\left(\lambda_{F2} - \lambda_{F1}\right)\left(\lambda_{F2} - \lambda_{\beta 1}\right)}{\left(\lambda_{F2} - \lambda_{\beta 2}\right)}\exp\left(\frac{-t}{\lambda_{F2}}\right) + \frac{\left(\lambda_{\beta 2} - \lambda_{\beta 1}\right)\left(\lambda_{\beta 2} - \lambda_{F1}\right)}{\left(\lambda_{\beta 2} - \lambda_{F2}\right)}\exp\left(\frac{-t}{\lambda_{\beta 2}}\right)\right]. \tag{12}$$

As per Fig. 8, this strain must be subtracted from the strain under constant applied stress (8). The remainder gives the strain corresponding to the creep recovery of Fig. 8a:

$$\gamma = -\dot{\gamma}_0\left[\lambda_{F1} + \lambda_{\beta 1} - \lambda_{F2} - \lambda_{\beta 2} + \frac{\left(\lambda_{F2} - \lambda_{F1}\right)\left(\lambda_{F2} - \lambda_{\beta 1}\right)}{\left(\lambda_{F2} - \lambda_{\beta 2}\right)}\exp\left(\frac{-t}{\lambda_{F2}}\right) + \frac{\left(\lambda_{\beta 2} - \lambda_{\beta 1}\right)\left(\lambda_{\beta 2} - \lambda_{F1}\right)}{\left(\lambda_{\beta 2} - \lambda_{F2}\right)}\exp\left(\frac{-t}{\lambda_{\beta 2}}\right)\right], \tag{13}$$

$$\gamma = \left[\lambda_{F1}^* + \lambda_{\beta 1}^* - \lambda_{F2}^* - \lambda_{\beta 2}^* + \frac{\left(\lambda_{F2}^* - \lambda_{F1}^*\right)\left(\lambda_{F2}^* - \lambda_{\beta 1}^*\right)}{\left(\lambda_{F2}^* - \lambda_{\beta 2}^*\right)}\exp\left(\frac{-\dot{\gamma}_0 t}{\lambda_{F2}^*}\right) + \frac{\left(\lambda_{\beta 2}^* - \lambda_{\beta 1}^*\right)\left(\lambda_{\beta 2}^* - \lambda_{F1}^*\right)}{\left(\lambda_{\beta 2}^* - \lambda_{F2}^*\right)}\exp\left(\frac{-\dot{\gamma}_0 t}{\lambda_{\beta 2}^*}\right)\right]. \tag{14}$$

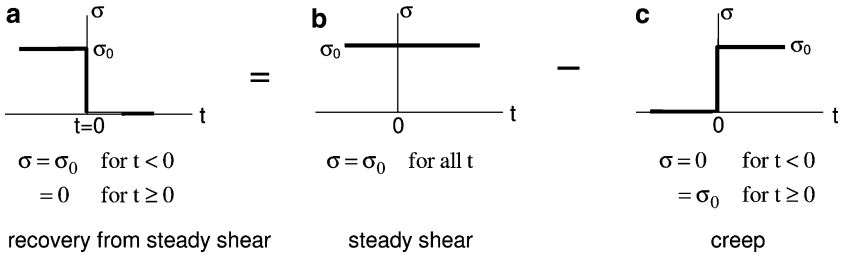

Fig. 8 Shear history of a recovery after cessation of steady shearing is depicted as a creep subtracted from steady shear

where we have also substituted $\sigma_0/\eta_b = \dot{\gamma}_0$. The negative sign simply indicates that the strain direction during recovery is opposite to that during retardation, and will be eliminated henceforth. For computational convenience, we reexpress the above equation in dimensionless terms using (26):

Thus, the ultimate recovery of the blend, obtained as $t \to \infty$, is given by

$$\gamma_\infty = \lambda^*_{F1} + \lambda^*_{\beta 1} - \lambda^*_{F2} - \lambda^*_{\beta 2} \tag{15}$$

i.e., the ultimate recovery is equal to the (sum of the dimensionless relaxation times) − (sum of dimensionless retardation times). We may consider this ultimate recovery to occur by two retardation processes: the "F" process, with a retardation time of λ_{F2}, and the "β" process with a retardation time of $\lambda_{\beta 2}$. The strains recovered by each of these processes are

$$\gamma_{\infty,F} = \frac{\left(\lambda^*_{F2} - \lambda^*_{F1}\right)\left(\lambda^*_{F2} - \lambda^*_{\beta 1}\right)}{\left(\lambda^*_{F2} - \lambda^*_{\beta 2}\right)} \tag{16}$$

and

$$\gamma_{\infty,\beta} = \frac{\left(\lambda^*_{\beta 2} - \lambda^*_{\beta 1}\right)\left(\lambda^*_{\beta 2} - \lambda^*_{F1}\right)}{\left(\lambda^*_{\beta 2} - \lambda^*_{F2}\right)}. \tag{17}$$

Model results

Equation 14 suggests that recovery can be characterized by five parameters: the two dimensionless retardation times λ^*_{F1} and $\lambda^*_{\beta 2}$, the strains $\gamma_{\infty,F}$ and $\gamma_{\infty,\beta}$ associated with each of the two processes, and finally the ultimate recovery $\gamma_\infty = \gamma_{\infty,F} + \gamma_{\infty,\beta}$. Since all the dimensionless times are proportional to the Ca (6), all these five parameters are proportional to Ca. These are plotted in Fig. 9a, b. Finally, examples of typical recovery curves at various values of β/α are plotted in Fig. 9c. All calculations in Fig. 9 have been done using $\phi = 0.1$, $p = 1$, and $\mathrm{Ca} = 0.4$, and only terms up to first order in ϕ have been retained for consistency with I.

Figure 9a shows that λ^*_{F2} approaches the retardation time for the blend without interfacial viscoelasticity (Eq. 9 in I) as β/α decreases. In contrast, the $\lambda^*_{\beta 2}$ retardation time increases with decreasing interfacial viscoelasticity; indeed, at low β/α, it can be shown that $\lambda^*_{\beta 2} \propto (\beta/\alpha)^{-1}$.

Figure 9b shows that at small β/α, $\gamma_{\infty,F}$ is equal to that for a blend without interfacial viscoelasticity (Eq. 10 in I):

$$\gamma_{\infty,\mathrm{uncompat}} = \mathrm{Ca}\,\frac{1}{80}\left(\frac{19p+16}{p+1}\right)^2\left[\phi - O(\phi^2)\right]. \tag{18}$$

$\gamma_{\infty,F}$ reduces sharply as β/α increases. In contrast, $\gamma_{\infty,\beta}$ has a more complex dependence on β/α: it can be shown that $\gamma_{\infty,\beta} \propto (\beta/\alpha)^{-1}$ at small β/α, but $\gamma_{\infty,\beta}$ is not monotonically decreasing as β/α increases.

Unlike the complex dependences of $\gamma_{\infty,F}$ and $\gamma_{\infty,\beta}$ on β/α, the total recovery γ_∞ has a very simple form: substituting the expressions for the λ_is in the Appendix into (15) and expanding at small ϕ, one obtains

$$\gamma_\infty = \lambda^*_{F1} + \lambda^*_{\beta 1} - \lambda^*_{F2} - \lambda^*_{\beta 2} = 5\mathrm{Ca}\phi\left(\frac{\alpha}{4\beta} + 1\right) + \mathrm{O}(\phi^2) \tag{19}$$

which is the monotonically decreasing function of β/α shown by the thick solid line in Fig. 9b. Remarkably, the total recovery is independent of viscosity ratio. This result is qualitatively consistent with Oldroyd's observation that if the interfacial modulus is frequency-independent, the blend viscosity η_b is equal to that of a suspension of rigid particles (and hence independent of p) (Oldroyd 1955). Furthermore, Fig. 9b shows that a blend with $\beta/\alpha > 0$ always shows greater recovery than a blend without interfacial viscoelasticity. This is also clear from comparing (19) and (18): the largest possible value of (18) is $19^2/80\mathrm{Ca}\phi = 4.51\mathrm{Ca}\phi$, which is always less than (19).

Finally, we note that the behavior of a blend with $\beta/\alpha \to 0$ is qualitatively different from one with $\beta/\alpha = 0$: even a small interfacial elasticity causes a new retardation process (albeit with a very long

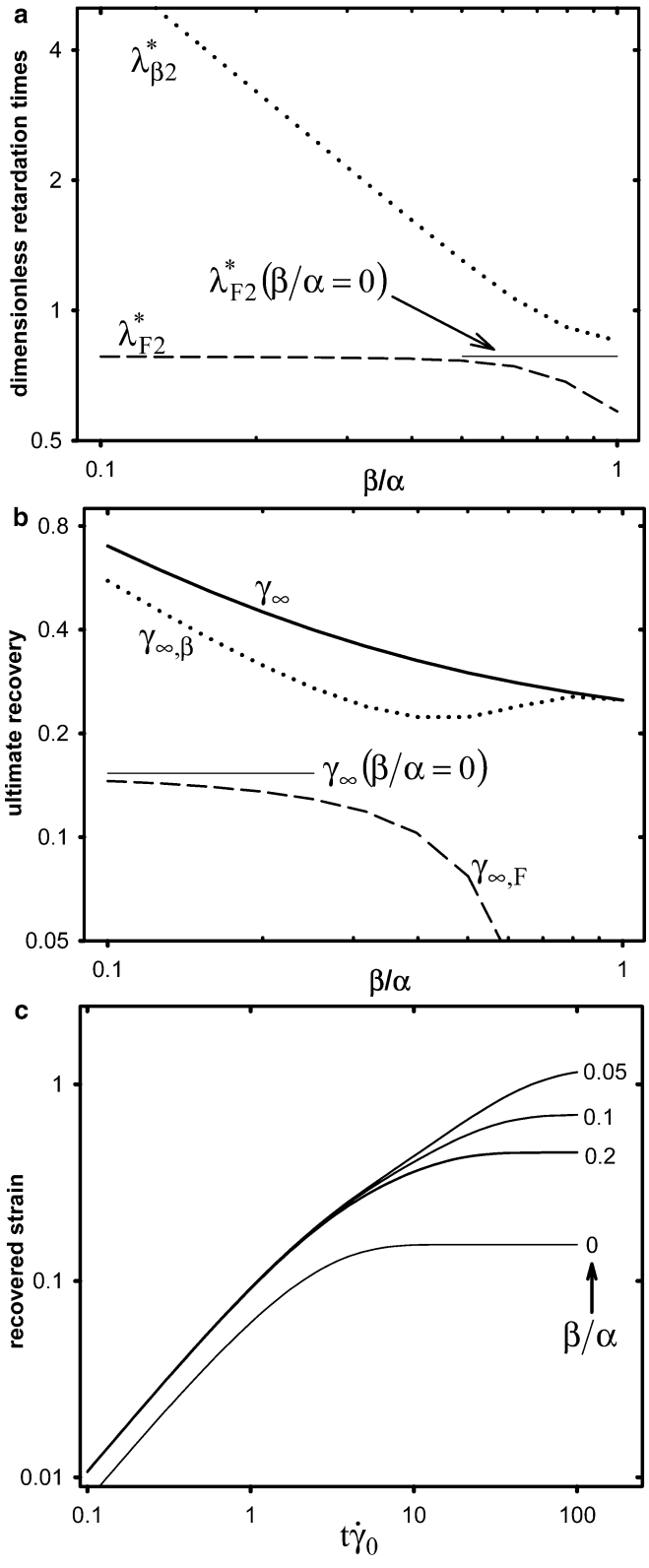

retardation time $\lambda^*_{\beta 2}$). Thus, as β/α increases from zero, γ_∞ first increases *discontinuously* and then decreases smoothly.

◀

Fig. 9 Dependence of recovery of blends with interfacial dilation modulus on β/α. All calculations use $\phi = 0.1$, $p = 1$, and $Ca = 0.4$, and all equations are used up to first order in ϕ. **a** Dimensionless retardation times (25, 26). The *horizontal line* is the blend without interfacial viscoelasticity (Eq. 9 from I). **b** Ultimate recovery, using (15, 16, 17). The *horizontal line* is the blend without interfacial viscoelasticity (18). **c** Recovery curves (14) for blends with interfacial dilation modulus, and Eq. 2 in I for the blend without interfacial viscoelasticity

Comparison with experimental results

Finally we compare the model predictions with experimental observations. The recovery for $\alpha/\beta = 0$ is a single retardation process. A small value of β/α changes the recovery curve abruptly due to the additional retardation process, while further increases in β/α cause gradual changes in the recovery curves. The shape of the sample recovery curves shown in Fig. 9c are similar to those observed in Fig. 2; in particular, the fact that recovery of compatibilized blends in Fig. 2 cannot be well represented by a single exponential function is captured by Fig. 9c. Yet, there is a serious qualitative discrepancy. With an increase in compatibilizer concentration, we expect the ratio β/α to increase; thus, the model suggests that the ultimate recovery should decrease with added compatibilizer. Exactly the opposite was observed experimentally. Furthermore, (19) predicts that the total recovery is independent of viscosity ratio, whereas a strong dependence on viscosity ratio was noted experimentally. We speculate on three possible causes of this discrepancy. The first, and perhaps most important, is that Fig. 9 examines the effects of interfacial viscoelasticity at constant Ca (fixed at 0.4), whereas there was certainly no means of ensuring that experimentally. Secondly, a time-independent β/α was assumed in the analysis. However, as drops retract during recovery, their area decreases, thus, increasing the compatibilizer concentration and increasing β/α. Lastly, the compatibilizer may not be distributed uniformly on the drop surfaces during the retraction process (as per the schematic in Fig. 7), whereas the model assumes uniform interfacial properties all over the drop. Indeed, since any steady flow is likely to cause significant gradients in compatibilizer concentration, this raises the question of whether a linear viscoelastic model can be rigorously applied to steady flow of compatibilized blends at all.

Summary and conclusions

The creep recovery after cessation of shear was examined for model compatibilized blends with droplet-matrix morphologies. Even small amounts of compatibilizer

were found to increase the ultimate recovery of the blends significantly. Addition of compatibilizer was also found to slow down the recovery process; however, in contrast with uncompatibilized blends, the recovery of compatibilized blends could not be captured by a single retardation process. Similar to blends without compatibilizer, the ultimate recovery was found to increase with increasing volume fraction of the drop phase and with decreasing viscosity ratio of the drops relative to the matrix. Finally, a limited number of transient creep experiments show that the compatibilizer increases the ultimate recovery under these conditions as well. In these experiments, a slow but weak retardation process was observed in compatibilized blends under some conditions.

All observations are consistent with a previously developed physical picture that accounts for flow-induced gradients in the compatibilizer concentration, and hence in interfacial tension, on the drop surfaces. However, the possible effects are wide-ranging, and in the absence of direct visualization, we are unable to comment on the exact mechanism that causes enhanced recovery. A constitutive approach that captures the compatibilizer effects in terms of interfacial viscoelasticity is able to capture the recovery kinetics qualitatively but shows significant quantitative disagreement with the data.

Acknowledgements We gratefully acknowledge the Laboratory of Applied Rheology at the Katholieke Universiteit Leuven for making the PIB-PMDS diblock copolymer available for this research. Funding for this research was provided by the University of Pittsburgh and by the Petroleum Research Fund of the ACS (Grant PRF# 39931-G9).

Appendix

The equations below are given by Jacobs et al. (1999). We correct a typographical error in those equations (Eq. 11 in Jacobs paper has $(1-(3/2)\,\phi)$ in the denominator whereas $(1+(3/2)\,\phi)$ is correct).

$$\lambda_{11}=\frac{R\eta_m}{\alpha}\frac{(19p+16)[2p+3-2\phi(p-1)]}{40(p+1)+2\frac{\beta}{\alpha}(23p+32)-2\phi\left[4(5p+2)+\frac{\beta}{\alpha}(23p-16)\right]} \tag{20}$$

$$\lambda_{12}=\frac{R\eta_m}{\alpha}\frac{\alpha}{\beta}\frac{40(p+1)+2\frac{\beta}{\alpha}(23p+32)-2\phi\left[4(5p+2)+\frac{\beta}{\alpha}(23p-16)\right]}{48(1-\phi)} \tag{21}$$

$$\lambda_{21}=\frac{R\eta_m}{\alpha}\frac{(19p+16)[2p+3+3\phi(p-1)]}{40(p+1)+2\frac{\beta}{\alpha}(23p+32)+3\phi\left[4(5p+2)+\frac{\beta}{\alpha}(23p-16)\right]} \tag{22}$$

$$\lambda_{22}=\frac{R\eta_m}{\alpha}\frac{\alpha}{\beta}\frac{40(p+1)+2\frac{\beta}{\alpha}(23p+32)+3\phi\left[4(5p+2)+\frac{\beta}{\alpha}(23p-16)\right]}{48(1+3\phi/2)}. \tag{23}$$

The relaxation and retardation times are given by

$$\begin{aligned}\lambda_{F1}&=2\lambda_{11}\left[1+\sqrt{1-4\frac{\lambda_{11}}{\lambda_{12}}}\right]^{-1};\\ \lambda_{\beta 1}&=2\lambda_{11}\left[1-\sqrt{1-4\frac{\lambda_{11}}{\lambda_{12}}}\right]^{-1}\end{aligned} \tag{24}$$

$$\begin{aligned}\lambda_{F2}&=2\lambda_{21}\left[1+\sqrt{1-4\frac{\lambda_{21}}{\lambda_{22}}}\right]^{-1};\\ \lambda_{\beta 2}&=2\lambda_{21}\left[1-\sqrt{1-4\frac{\lambda_{21}}{\lambda_{22}}}\right]^{-1}.\end{aligned} \tag{25}$$

Equations 24 and 25 are in a slightly different algebraic form than those provided by Jacobs et al. (1999): since λ_{11} and λ_{21} both remain finite in the limit of $\beta/\alpha=0$, (24) and (25) are slightly more convenient than those given by Jacobs et al. Finally, all the above times can be made dimensionless by multiplying by the steady shear rate $\dot{\gamma}_0$:

$$\lambda^*_{F1}=\dot{\gamma}_0\lambda_{F1};\quad \lambda^*_{\beta 1}=\dot{\gamma}_0\lambda_{\beta 1};\quad \lambda^*_{F2}=\dot{\gamma}_0\lambda_{F2};\quad \lambda^*_{\beta 2}=\dot{\gamma}_0\lambda_{\beta 2}. \tag{26}$$

References

Edwards DA, Brenner D, Wasan DT (1991) Interfacial transport processes and rheology. Butterworth-Heinemann, Boston

Jacobs U, Fahrländer M, Winterhalter J, Friedrich C (1999) Analysis of Palierne's emulsion model in the case of viscoelastic interfacial properties. J Rheol 43:1497–1509

Li X, Pozrikidis C (1997) The effect of surfactants on drop deformation and on the rheology of dilute emulsions in Stokes flow. J Fluid Mech 341:165–194

Luciani A, Champagne MF, Utracki LA (1997) Interfacial tension coefficient from the retraction of ellipsoidal drops. J Polym Sci Part B Polym Phys 35:1393–1403

Milliken WJ, Leal LG (1994) The influence of surfactant on the deformation and breakup of a viscous drop: The effect of surfactant solubility. J Colloid Interface Sci 166:275–285

Oldroyd JG (1953) The elastic and viscous properties of emulsions and suspensions. Proc R Soc Lond A218:122–132

Oldroyd JG (1955) The effect of interfacial stabilizing films on the elastic and viscous properties of emulsions. Proc R Soc Lond A232:567–577

Palierne JF (1990) Linear rheology of viscoelastic emulsions with interfacial tension. Rheol Acta 29:204–214

Pawar Y, Stebe K (1996) Marangoni effects on drop deformation in an extensional flow: the role of surfactant physical chemistry. 1. Insoluble surfactants. Phys Fluids 8:1738–1751

Riemann RE, Cantow HJ, Friedrich C (1997) Interpretation of a new interface-governed relaxation process in compatibilized polymer blends. Macromolecules 30:5476–5484

Stone HA, Leal LG (1990) The effects of surfactants on drop deformation and breakup. J Fluid Mech 220:161–186

Van Hemelrijck E, Van Puyvelde P, Velankar S, Macosko CW, Moldenaers P (2004) Interfacial elasticity and coalescence suppression in compatibilized polymer blends. J Rheol 48:143–158

Van Puyvelde P, Velankar S, Mewis J, Moldenaers P (2002) Effect of Marangoni stresses on the deformation and coalescence in compatibilized immiscible polymer blends. Polym Eng Sci 42:1956–1964

Velankar S, Van Hemelrijck E, Van Puyvelde P, Moldenaers P, Macosko CW (2001a) Shear-induced coalescence in compatibilized polymer blends. In: Proceedings of the 3rd Pacific Rim Conference on Rheology

Velankar S, Van Puyvelde P, Mewis J, Moldenaers P (2001b) Effect of compatibilization on the breakup of polymeric drops in shear flow. J Rheol 45:1007–1019

Velankar S, Van Puyvelde P, Mewis J, Moldenaers P (2004a) Steady-shear rheological properties of model compatibilized blends. J Rheol 48:725–744

Velankar S, Zhou H, Jeon HK, Macosko CW (2004b) CFD evaluation of drop retraction methods for the measurement of interfacial tension of surfactant-laden drops. J Colloid Interface Sci 272:172–185

Vinckier I, Mewis J, Moldenaers P (1999a) Elastic recovery of immiscible blends 2.Transient flow histories. Rheol Acta 38:198–205

Vinckier I, Moldenaers P, Mewis J (1999b) Elastic Recovery of immiscible blends 1. Analysis after steady state shear flow. Rheol Acta 38:65–72